第 48 卷第 4 期
2020 年 4 月

硅 酸 盐 学 报
JOURNAL OF THE CHINESE CERAMIC SOCIETY

Vol. 48，No. 4
April，2020

http://www.gxyb.cbpt.cnki.net

DOI：10.14062/j.issn.0454-5648.20190642

基于 TiO_2/多壁碳纳米管复合光阳极和 SnO_2/多壁碳纳米管非铂对电极的染料敏化太阳能电池电子传输的改善

刘青龙，王晓宇，赵丽萍，金立国

(哈尔滨理工大学材料科学与工程学院，哈尔滨 150040)

摘　要：为了提高 TiO_2 光阳极的电子传输速率，在 TiO_2 中负载了多壁碳纳米管(MWCNTs)。采用溶胶–凝胶水热法制备了 TiO_2/MWCNTs 复合溶胶，利用电流体动力学方法制备了均匀的 TiO_2/MWCNTs 复合薄膜，并用 $TiCl_4$ 对薄膜进行了优化。用扫描电子显微镜、透射电子显微镜、X 射线衍射仪和紫外可见吸收光谱仪对样品进行了表征分析。利用电化学阻抗谱和电流密度–电压曲线分析了基于 TiO_2/MWCNTs 复合光阳极和 SnO_2/MWCNTs 对电极的染料敏化太阳能电池(DSSC)的光电性能。结果表明，MWCNTs 的加入极大地加速了电子在薄膜中的传输，减少了电子与氧化态染料和 I_3^-的复合；基于 CNT-0.12(质量分数 0.12%)复合光阳极的 DSSC 性能最佳(V_{OC}=0.70 V，J_{SC}=13.0 mA/cm^2，η_{FF}=0.64，η=5.80%)，与基于纯 TiO_2 光阳极的 DSSC(η=4.44 %)相比，能量转换效率提高了 30.6%。

关键词：光阳极；多壁碳纳米管；染料敏化太阳能电池；电流体动力学
中图分类号：TM914　**文献标志码**：A　**文章编号**：0454–5648(2020)04–0483–08
网络出版时间：2020–01–14



Improvement of Electron Transport in Dye-Sensitized Solar Cells Based on TiO_2/MWCNTs Composite Films as a Photoanode and SnO_2/MWCNTs as a Pt-free Counter Electrode

LIU Qinglong, *WANG Xiaoyu*, *ZHAO Liping*, *JIN Liguo*
(School of Materials Science and Engineering, Harbin University of Science and Technology, Harbin 150040, China)

Abstract: In order to improve the electron transport rate of TiO_2 photoanode, multi-walled carbon nanotubes (MWCNTs) were loaded in TiO_2. TiO_2/MWCNTs composite sols were formed by a sol–gel hydrothermal method, and the uniform TiO_2/MWCNTs composite films were formed by an electro-hydrodynamic method. The films were optimized with $TiCl_4$. The samples were characterized by scanning electron microscopy, transmission electron microscopy, X-ray diffractometer and ultraviolet–visible absorption spectroscopy. The photoelectric properties of dye-sensitized solar cells (DSSCs) based on TiO_2/MWCNTs composite photoanodes and SnO_2/MWCNTs counter electrode were analyzed by electrochemical impedance spectroscopy and current density–voltage curve measurement. The results show that the addition of MWCNTs considerably accelerates the transport of electrons in the films and decreases the recombination of electrons with oxidized dye and I_3^-; The DSSC with a CNT-0.12 (0.12%, in mass) composite photoanode shows the optimal performance (*i.e.*, V_{oc}=0.70 V, J_{sc}=13.0 mA/cm^2, η_{FF}=0.64, η=5.80%), and the power conversion efficiency is 30.6% greater than that of DSSC with a pure TiO_2 photoanode (*i.e.*, η=4.44%).

Keywords: photoanode; multi-walled carbon nanotubes; dye-sensitized solar cells; electrohydrodynamics

1 Introduction

Environmental and energy issues are the two major problems facing the world today. As an inexhaustible new energy source, solar energy has received extensive attention[1], and the equipment needed to convert solar energy into usable energy are solar cells. At present, the most widely used solar cells are mainly silicon solar cells,

收稿日期：2019–09–20。　修订日期：2019–11–24。
基金项目：国家自然科学基金(21273060)。
第一作者：刘青龙(1995—)，男，硕士研究生。
通信作者：金立国(1971—)，男，博士，教授。

Received date: 2019–09–20.　**Revised date:** 2019–11–24.
First author: LIU Qinglong (1995–), male, Master candidate.
E-mail: 774882853@qq.com
Correspondent author: JIN Liguo (1971–), male, Ph.D., Professor.
E-mail: jinliguo@hrbust.edu.cn

but their high cost limits their wide application. Since O'regan et al.[2] prepared dye-sensitized solar cells (DSSCs) with TiO_2 nanocrystal film-adsorbed dye as a photoanode in 1991, DSSCs have attracted much attention from researchers. The manufacturing cost of dye-sensitized solar cells is only 1/5–1/10 of the cost of silicon solar cells[3], and it also has the advantages of a wide range of raw materials, simple manufacturing process and high theoretical efficiency. A typical dye-sensitized solar cell consists of a photoanode, electrolyte and counter electrode. The working process of the cell is that the dye molecules adsorbed on the semiconductor film receive solar energy. Then, the electrons are excited from the highest occupied molecular level (HOMO) to the lowest unoccupied molecular level (LUMO). The excited state electrons are injected into the conduction band of TiO_2. The electrons in the conduction band reach the external circuit through a conductive glass substrate, and at the same time, the oxidized dye molecules are regenerated by I^- reduction with a reducible electrolyte. I_3^- receives electrons from the Pt counter electrode and is reduced into I^-, and thus, a current cycle in the dye-sensitized solar cells is completed[4]. The photoanode plays a role in absorbing dyes and collecting and transporting photogenerated electrons, which have a great influence on the efficiency of the cells[5].

TiO_2 is the most widely used semiconductor material in photoanodes[6]. However, the improvement of conversion efficiency has reached a bottleneck period for dye-sensitized solar cells with a single TiO_2 structure. The accumulation of disordered TiO_2 nanoparticles has many poor uneven interfaces and a large charge transfer resistance, resulting in the recombination of a large number of electrons and electrolytes, which greatly reduces the energy conversion efficiency of cells. At the same time, the electron transport property of TiO_2 is weaker than that of other semiconductor materials, such as ZnO and SnO_2[7–8]. However, it can be improved by combining other stable materials with TiO_2[9–11]. Some researchers have also attempted to replace TiO_2 nanoparticles with one-dimensional TiO_2 nanostructures, such as nanotubes[12–13], nanowires[14] and nanorods[15–16], to provide direct electron transport channels.

Carbon nanotubes (CNT) have attracted extensive attention owing to their excellent mechanical properties, electron transport, electrical conductivity, thermal conductivity and catalytic properties[17–18]. CNT is widely used as one-dimensional nanomaterials in photocatalysis, solar cells, sensors, pharmaceuticals, transistors, batteries and other fields[19–24]. Kilic et al.[25]. used a hydrothermal method to grow TiO_2 on conductive glass with multiwalled carbon nanotubes MWCNTs arranged vertically to prepare TiO_2/MWCNTs composite photoanodes. Finally, the cell was assembled with a Fe_2S counter electrode and obtained a conversion efficiency of 7.27%. Yu et al.[26]. compounded TiO_2 hollow nanospheres with MWCNTs by mechanical stirring and a doctor blade method, which finally improved the conversion efficiency by 3.94% compared with that of a pure TiO_2 film. It has also been noted that CNT loading greatly affects the structure of the thin film and the conversion efficiency of the battery. Du et al.[27] used electrospinning technology to prepare TiO_2/MWCNTs hybrid nanofiber films as the photoanode for DSSCs and obtained a conversion efficiency of 5.63% at an appropriate CNT content. The author believed that excessive CNT addition would lead to agglomeration and an excessive reduction of the downward shift in Fermi level of the composite photoanode. Therefore, the combination of CNT and a semiconductor oxide is an effective method to improve the conversion efficiency.

The role of the DSSCs counter electrode (CE) is to catalyze effective reduction of the oxidized electrolyte. The perfect counter electrode should exhibit excellent electrocatalytic activity, high electrical conductivity, and good durability in redox electrolytes[28]. Pt, as a kind of catalytic material, has been widely used in DSSCs, but because of its diminishing reserve and high price, its application in DSSCs is limited. Thus, it is necessary to explore Pt-free CE materials. Many researchers have devoted themselves to the study of Pt-free materials. At present, some materials show the same catalytic performance as Pt, such as a porous Co_3S_4/MoS_2 nanostructure[29], a $Co_{0.5}Ni_{0.5}Se$/graphene nanohybrid[30], carbon black/graphite powers[31] and a NiS/MWCNTs composite[32].

At present, the most widely used methods for film preparation are the doctor blade method, screen printing and spin coating, which have the disadvantages of a complicated operation, an unevenly applied thickness and a difficult to control thickness. Electrohydrodynamics (EHD) has a wide application in the preparation of nanomaterials; it is a technology of breaking a solution or sol with a certain viscosity into microdroplets or microjets under the action of a high voltage direct current electric field and spraying them on a substrate to form a thin film. EHD can be divided into electrospinning and electrospraying according to the prepared material characteristics. Electroelectrospinning is mainly applied toward the preparation of nanofibers, and electrospraying is used to prepare nanoparticles. Different nanomaterials can be prepared by changing the viscosity and the electric conductivity of the sprayed liquid. The films obtained by applying the above technology have the advantages of a high and uniform porosity, uniform thickness and thickness that can be controlled by the amount of sol used for spraying.

In a previous study, we explored the catalytic

performance of the SnO_2/MWCNTs counter electrode and found that the catalytic performance of the SnO_2/MWCNTs was comparable to Pt[32]. In the present research, TiO_2/MWCNTs composite sols were synthesized by a sol–gel hydrothermal method. Mesoporous TiO_2/MWCNTs composite photoanode film with a uniform thickness was obtained by EHD. TiO_2/MWCNTs composite photoanodes and SnO_2/MWCNTs composite counter electrodes were assembled into DSSCs, and the effect of the MWCNTs content in the photoanodes on the performance of the DSSCs was investigated.

2 Experimental

2.1 Preparation of the TiO_2/MWCNTs solution

To obtain a uniformly dispersed TiO_2/MWCNTs composite solution, specific amounts of carboxylated MWCNTs were dispersed in 3 mL of an aqueous solution containing 0.03 g sodium dodecyl benzene sulfonate and sonicated until the MWCNTs were uniformly dispersed. TiO_2 solution was prepared by a slow dropwise addition of 4.625 mL titanium tetraisopropoxide (TTIP) in a mixed solution of 31.25 mL deionized water, 10 mL alcohol and 0.25 mL isopropyl alcohol and stirred until clear in an ice-water bath. The TiO_2/MWCNTs composite gel was obtained by adding the MWCNTs solution into the TiO_2 solution and stirring at 80 ℃ for 8 h. Then, the gel was condensed to a certain concentration by rotary evaporation. The gel was placed into a polytetrafluoroethylene high-pressure hydrothermal reactor and heated at 180 ℃ for 12 h to obtain a sol. The mixed sol for EHD was prepared by ultrasonic treatment for 1 h with adding a certain amount of polyvinyl alcohol (PVA) into the mixed solution of hydrothermal sol, ethanol and deionized water.

2.2 Preparation of TiO_2/MWCNTs nanocomposite films

The F-doped SnO_2-coated glass (FTO glass, 14 Ω/sq) was ultrasonically cleaned with detergent, deionized water, acetone, ethanol and deionized water for 10 min, respectively. The compact TiO_2 film was obtained by spin-coating method with a butyl titanate ethanol solution, which can prevent the recombination of photoinjected electrons with electrolyte at the FTO/TiO_2 interface and improve the adherence between the TiO_2/MWCNTs porous layer and the FTO conductive substrate. The prefabricated films on the conductive substrates with an active area of 2 cm^2 were prepared by spraying a certain amount of TiO_2/MWCNTs sols with EHD. A schematic diagram of the EHD is shown in Fig. 1. The prefabricated films were sintered at 500 ℃ for 2 h under N_2 protection, cooled to room temperature, and then immersed into 0.2 mol/L $TiCl_4$ solution at 70 ℃ for 2 h; next, they were washed with deionized water and dried in air. Finally, the TiO_2/MWCNTs composite photoanode films were sintered at 500 ℃ for 2 h under N_2 protection. Six samples were prepared and named CNT-w (w=0, 0.04, 0.08, 0.12, 0.16, 0.20), where w was the mass fraction of MWCNTs to TiO_2.

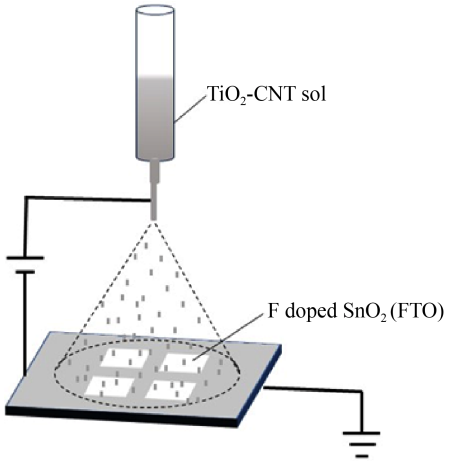


Fig. 1　Schematic diagram of the electrohydrodynamic technology

2.3 Preparation of the SnO_2/MWCNTs composite CE

In a typical experiment, SnO_2/MWCNTs composite films were prepared according to the method reported in our previous work[33]. Briefly, 40 mg MWCNTs were ultrasonically dispersed in 40 mL deionized water. A small amount of concentrated hydrochloric acid and 1.55 g $SnCl_4 \cdot 5H_2O$ were mixed in, and then ammonia was added dropwise until the pH was 9. Then, the solution was subjected to a hydrothermal reaction at 180 ℃ for 18 h. The composite was obtained by washing repeatedly with deionized water and ethanol and dried at 60 ℃ for 24 h. The SnO_2/MWCNTs composite films were prepared on the FTO glass by EHD. The films were annealed at 500 ℃ for 2 h under N_2 protection.

2.4 Assembly of the DSSCs and their characterization

The obtained composite films were soaked in an ethanol solution of 0.3 mmol/L ruthenium complex (N719) for 24 h after heating to 100 ℃. The photoanodes were rinsed with ethanol to remove excess dye that was not adsorbed and dried. SnO_2/MWCNTs were used as counter electrodes in this experiment. The electrolyte was prepared by dissolving 0.1 mol/L lithium iodide, 0.05 mol/L iodine and 0.45 mol/L 1-methyl-benzimidazole in 3-methoxy propionitrile and 1-propyl-3-methyl imidazole solution. The photoanode, electrolyte and counter electrode were assembled into a sandwich structure to obtain DSSCs with an area of 0.2 cm^2. A schematic diagram of an assembled DSSC is shown in Fig. 2.

Scanning electron microscopy (SEM, FEI Sirion 200, Shimadzu, Japan) and transmission electron microscopy (TEM, JEM-2100, Japan Electronics Co.

Ltd., Japan) were used to analyze the morphology of the composite film. The crystal structures of the materials were characterized by X-ray diffraction (XRD, D/max-3B, PANalytical B.V., Holland). A Raman spectrometer (HR 800, France HORIBA Jobin Yvon, France) was used to record the Raman spectra of the composite materials. The specific surface areas of photoanode and counter electrode were measured by specific surface area tester (ST-08, Shandong Sangze Instrument Co. Ltd. China). The optical absorbance spectra of the photoanodes was recorded with ultraviolet visible spectrometer (UV-Vis, USB-4000, Ocean Optics, America), and spectrophotometer (722N, Shanghai Precision Science and Technology Co. Ltd., China) was used to measure the dye absorption of the photo-anode. Under the condition of illumination intensity of 100 mW/cm^2 (AM 1.5), the photoelectric performance of the DSSCs was tested and analyzed by using electrochemical workstation (RST 5000, RST Co. Ltd., China). The electrochemical impedance analysis (EIS) was measured in dark conditions *via* electrochemical workstation (RST 5000, RST Co. Ltd., China).

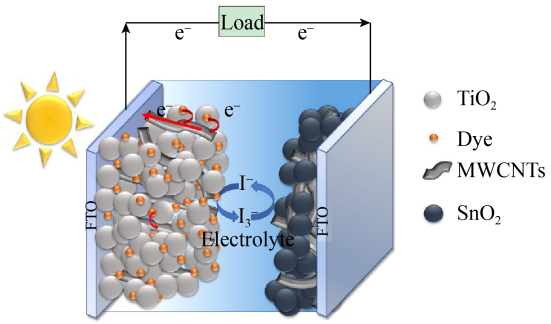


Fig. 2 Schematic diagram of dye-sensitized solar cells (DSSCs)

3 Results and discussions

3.1 Morphology and Crystal Structure

Fig. 3 shows the SEM images of the surface and cross-section morphology of CNT-0 and CNT-0.12 composite photoanode films which were treated by $TiCl_4$. As observed in Figs. 3(a) and 3(c), the thickness of the prepared composite films is relatively uniform, and the average thickness are both approximately 10 μm, which is more favorable for electron transmission and solar light scattering. The morphology of CNT-0.12, as shown in Fig. 3(c), exhibits more pores in the film. The increase of mesopores is more conducive to the adsorption of dye and the penetration of electrolyte. The above increases the utilization rate of sunlight and accelerates the generation of electrons, thus improving the conversion efficiency of the DSSCs. In Figs. 3(b) and 3(d), many porous structures and agglomerated TiO_2 nanoparticles can also be seen on the surface of the thin film. However, MWCNTs are not observed on the surface, which may be due to the low content of MWCNTs and the treatment of the thin film with $TiCl_4$, resulting in the MWCNTs on the surface being covered. Fig. 4 shows TEM images of the annealed CNT-0 and CNT-0.12 composite photoanodes. The size of the prepared TiO_2 nanoparticles is uniform. It is quite clear from the TEM images in Fig. 4b that many TiO_2 particles are anchored on the outer surface of the long tubular MWCNTs, and this assembly ensures efficient electron transport through the CNTs. Fig. 5 shows SEM images of the cross-section morphology of the SnO_2/MWCNT counter electrode. The composite film has a uniform porous structure, which is beneficial for increasing the catalytic active surface area of the electrode and improving the contact between the electrode and the electrolyte. The average thickness is approximately 6.5 μm.

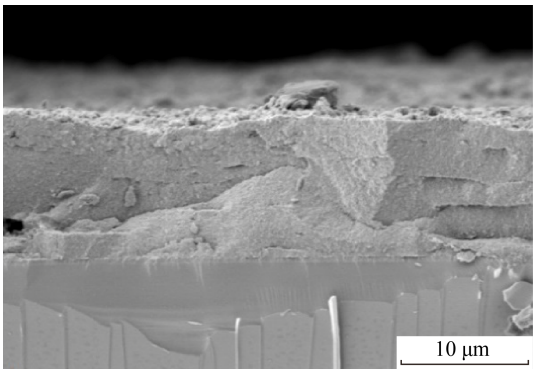
The specific surface area of the composite powders scraped from the CNT-0.12 and SnO_2/MWCNTs composite films were measured by a specific surface area tester. The specific surface area of CNT-0.12 and SnO_2/MWCNTs composite films are 84 and 114 m^2/g, respectively. The larger specific surface area of SnO_2/MWCNTs is more beneficial for dye adsorption and the catalysis of electrolytes for photoanodes and counter electrodes.

XRD patterns of TiO_2/MWCNTs composite films after heat treatment at 500 ℃ are shown in Fig. 6. For all films, obvious diffraction peaks are observed at 2θ=25.3°, 37.8°, 48.0°, 53.9°, 55.0° and 62.7°. These peaks respectively correspond to the (101), (004), (200), (102), (211), (204) crystal planes of anatase TiO_2 (JCPDS 84-1285). There are obvious diffraction peaks at 2θ=26.6° and 65.7° for TiO_2/MWCNTs composite films with MWCNTs contents of 0.04%, 0.08%, and 0.12%. These peaks correspond to SnO_2 (JCPDS 46-1088), which is mainly caused by SnO_2 on the glass substrate. However, no obvious MWCNTs characteristic peaks are observed in the XRD diffraction peak. This may be due to the low MWCNTs content and the overlapping positions of the characteristic diffraction peak of MWCNTs at 26.0° and the main peak of anatase TiO_2 at 25.3°. This is similar to the results reported in the previous literatures[26, 34].

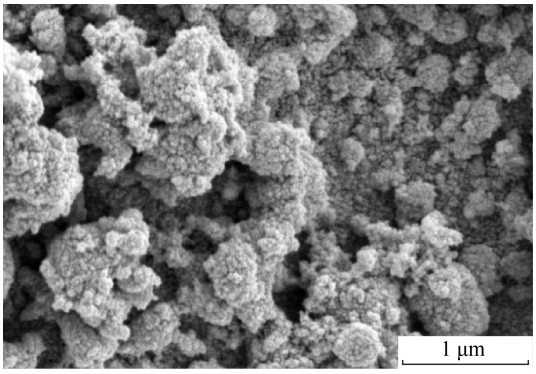
3.2 Raman Spectra

To confirm the existence of MWCNTs, Raman spectra of the prepared composite films were characterized. As shown in Fig. 7, the Raman spectra of carboxylated MWCNTs, annealed TiO_2 and TiO_2/MWCNTs composite films were recorded at an excitation wavelength of 514.5 nm. Strong vibration peaks at 143, 395, 516 and 636 cm^{-1} can be observed for the pure TiO_2 samples. They correspond to the vibrational modes of E_g, B_{1g}, A_{1g} and E_g of anatase TiO_2, respectively. For the acid-treated MWCNTs,

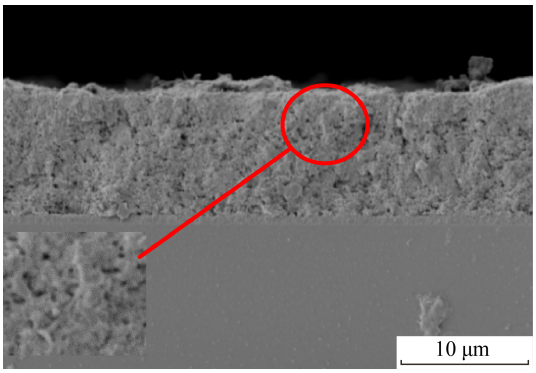
obvious characteristic peaks appear at 1 359 and 1 579 cm^{-1} that are assigned to the structural disorder D band and tangential vibrational G band of MWCNTs[35].



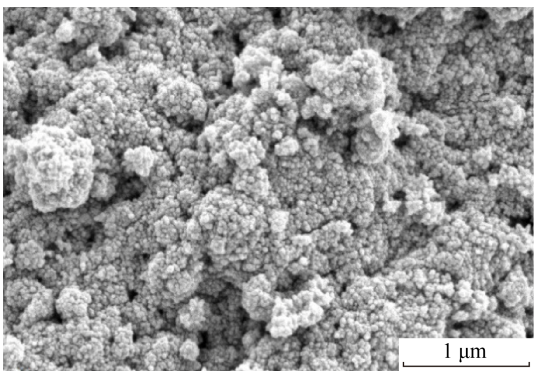
(a) Cross-section image of CNT-0



(b) Surface image of CNT-0

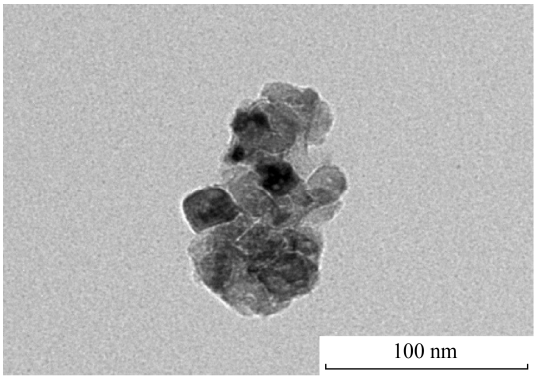


(c) Cross-section image of CNT-0.12

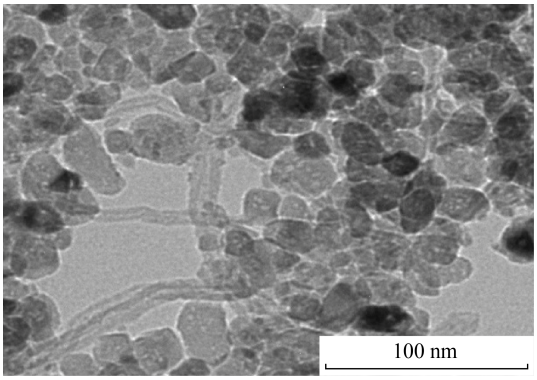


(d) Surface image of CNT-0.12

Fig. 3　SEM images of different MWCNTs contents loaded in TiO_2



(a) CNT-0



(b) CNT-0.12

Fig. 4　TEM images of different MWCNTs contents loaded in TiO_2

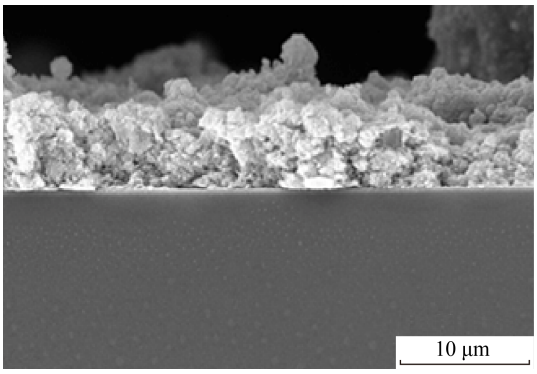


Fig. 5　Cross-section SEM image of SnO_2/MWCNTs

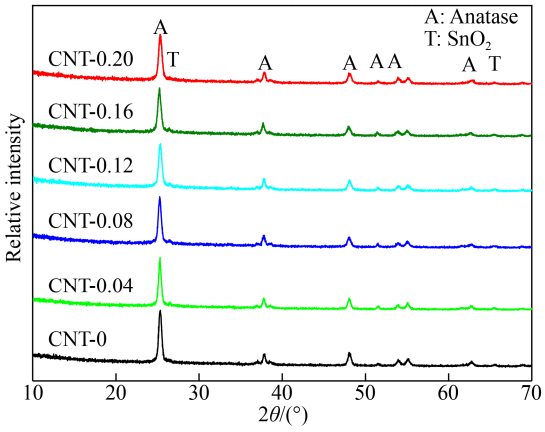


Fig. 6　XRD spectra of different TiO_2/MWCNTs composite films

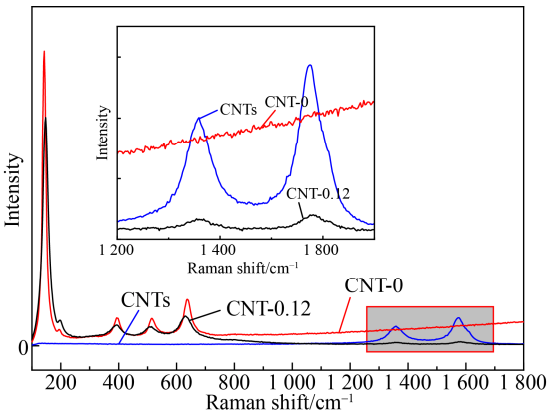


Fig. 7 Raman spectra of the MWCNTs, annealed pure TiO_2 (CNT-0) and composite film (CNT-0.12) and a magnified view of the respective spectra in a range of 1 200–1 700 cm^{-1}

Two weak characteristic peaks at 1 354 cm^{-1} and 1 575 cm^{-1} are observed besides the characteristic peaks of anatase TiO_2 in the TiO_2/MWCNTs composites, which are mainly caused by the MWCNTs. The Raman results confirm the existence of MWCNTs in the composite film.

3.3 UV-Vis analysis

Fig. 8 shows the optical absorbance spectra of different photoanodes after dye adsorption. Compared with the TiO_2 photoanode (CNT-0), the photoanodes with a small amount of MWCNTs loading (CNT-0.04, CNT-0.08, CNT-0.12) have obviously increased absorption intensity at wavelengths higher than 500 nm. The TiO_2 photoanode has a strong absorption peak at approximately 515 nm. With increasing MWCNTs content, the absorption peak gradually moves to a longer wavelength. However, the absorption intensity gradually decreases. To further investigate the effect of MWCNTs loading on dye adsorption, TiO_2/MWCNTs composite photoanodes that had adsorbed dye were soaked in 0.1 mol/L NaOH and ethanol solution for 24 h. The absorbance of the desorption solution was tested at 515 nm by a spectrophotometer, and the dye adsorption of the photoanode was calculated by Beer-Lambert law. The calculation results are listed in Table 1. The comparison shows that the dye adsorption is improved to a certain extent by loading a proper amount of MWCNTs, and the dye loading in the CNT-0.12 photoanode reaches a maximum of 7.72×10^{-8} mol/cm^2. The dye adsorption decreases with a further increase in MWCNTs loading. This may be due to the reduction of contact area between the TiO_2 and dye caused by an excessive amount of MWCNTs. However, a proper amount of MWCNTs loading can increase the porosity of TiO_2, thus increasing dye penetration and adsorption. This is also shown in the SEM results.

3.4 Electrochemical Impedance Spectroscopy

Electrochemical impedance spectroscopy (EIS) analysis is widely used with DSSCs to study electron and ionic reactions. Generally, a Nyquist plot includes three semicircles, of which the semicircle in the high frequency region represents charge transfer at the counter electrode, the intermediate frequency region indicates electron transfer and transmission at the TiO_2/dye/electrolyte interface, and the low frequency region represents the Warburg diffusion process of I^-/I_3^- in the electrolyte[36]. To further study the influence of the MWCNTs addition on electron and ion transport, electrochemical impedance measurements were carried out in dark conditions by applying a bias of the open circuit voltage, with an alternative current amplitude of 20 mV at a frequency range between 100 mHz and 100 kHz. Equivalent circuit modeling was performed using Z View software. Fig. 9 shows the semicircles of the intermediate frequency region of the Nyquist plots of a DSSC assembled with TiO_2/MWCNTs composite photoanodes. The equivalent circuit model is inserted into Fig. 9. The parameters obtained are listed in Table 1. R_1 is the series resistance. R_2 indicates the electrochemical reaction resistance that takes place at the photoanode. The larger the value of R_2, the smaller the probability of electron recombination occurring at TiO_2[36–37]. From the Table 1, we can see that the addition of MWCNTs reduces the series resistance (R_1) of the DSSCs, and the CNT-0.12 electrode has the smallest R_1, which indicates that the addition of MWCNTs accelerates the transmission of electrons. At the same time, R_2 has a larger value with increasing MWCNTs content, which further shows that the enhancement in photocurrent density can be attributed to the decrease in the recombination rate of electrons. However, R_2 has a downward trend when the MWCNTs content exceeds 0.12% (in mass). This may be due to a slow charge transfer caused by more MWCNTs entanglement and accumulation, thus increasing the probability of electron recombination.

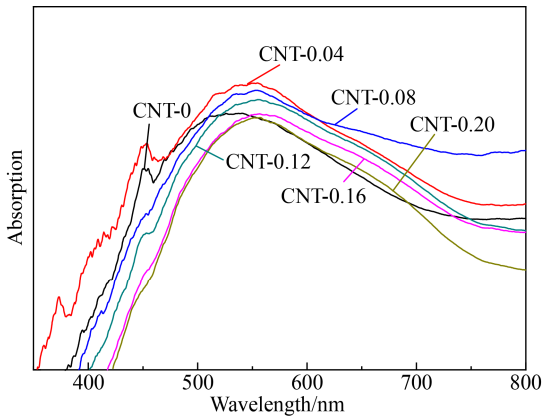
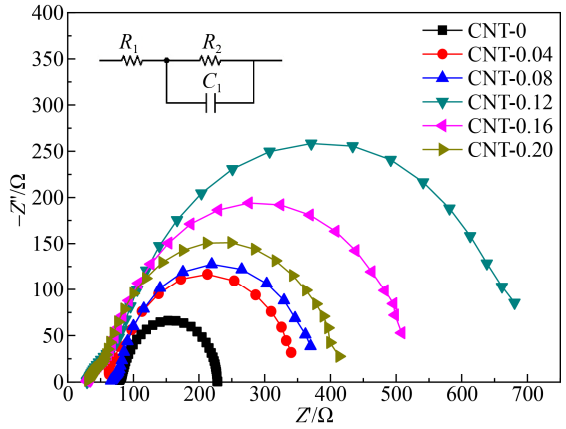


Fig. 8 Absorption spectra of different TiO_2/MWCNTs composite films after adsorbing N719

Table 1　Electrochemical impedance spectroscopy analysis parameters and the amount of adsorbed dye

Sample	w(MWCNTs)/%	R_1/Ω	R_2/Ω	c(absorbed dye)×10^8/(mol·cm^{-2})
CNT-0	0.00	81.81	106.7	3.98
CNT-0.04	0.04	66.68	254.9	4.86
CNT-0.08	0.08	77.38	275.2	6.77
CNT-0.12	0.12	38.35	503.5	7.72
CNT-0.16	0.16	39.06	388.1	6.77
CNT-0.20	0.20	40.65	314.6	3.39

R_1 is the series resistance; R_2 is the electrochemical reaction resistance.



C_1 describes capacitance of porous electrodes.

Fig. 9　Nyquist plots of the DSSCs based on different composite electrodes

3.5　Photocurrent-voltage characteristics

The current density–voltage (J–V) curves of DSSCs assembled with TiO_2/MWCNTs composite electrodes containing different MWCNTs contents are shown in Fig. 10, and other parameters related to solar cells are listed in Table 2. It can be clearly seen that the appropriate addition of MWCNTs improves the open circuit voltage (V_{oc}) and short circuit current (J_{sc}) of the DSSCs, in which V_{oc} increases from 0.69 V to 0.70 V and J_{sc} increases from 11.3 mA/cm^2 to 13.0 mA/cm^2. The high open circuit voltage obtained is mainly related to the low back electron transfer rate. The addition of MWCNTs provides a direct electron transfer channel. The residence time of electrons is reduced, and the probability of recombination with oxidized electrolyte is further decreased. The improvement of the short-circuit current is mainly due to the faster electron transport rate of MWCNTs. A small amount of MWCNTs loading accelerates electron transportation and collection. Compared with 4.44% of the pure TiO_2, the power conversion efficiency of DSSC based on the TiO_2/MWCNTs (0.12%) composite photoanode reaches 5.80% (30.6% higher than that of CNT-0). This improved conversion efficiency benefits from the reduction of the electron recombination rate and the increase of dye adsorption. However, with the increase of MWCNTs contents, the conversion efficiency decreases instead. This may be due to the entanglement and accumulation of MWCNTs in the photoanode, which affect the transmission of electrons. The increase of MWCNTs leads to a reduction in light absorption. This causes the short-circuit current density to decrease.

Table 2　Photovoltaic parameters of DSSCs based on TiO_2/MWCNTs composite films

Samples	w(MWCNTs)/%	J_{SC}/(mA·cm^{-2})	V_{OC}/V	η_{FF}	η/%
CNT-0	0.00	11.3	0.69	0.58	4.44
CNT-0.04	0.04	10.4	0.69	0.66	4.72
CNT-0.08	0.08	11.2	0.70	0.67	5.22
CNT-0.12	0.12	13.0	0.70	0.64	5.80
CNT-0.16	0.16	11.8	0.70	0.65	5.38
CNT-0.20	0.20	12.5	0.68	0.63	5.29

η_{FF} is fill factor; η is energy transfer efficiency.

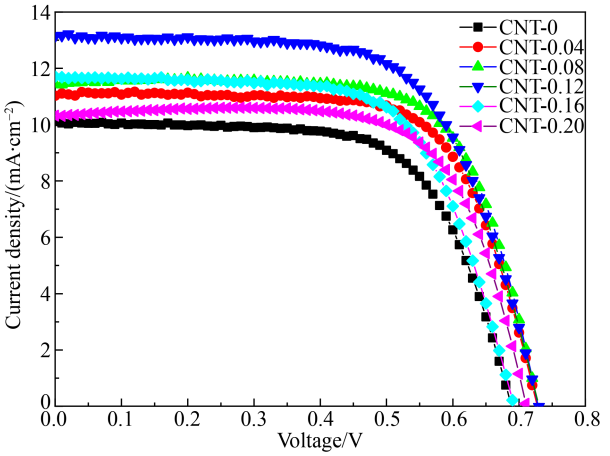


Fig. 10　J–V curves of the DSSCs assembled with TiO_2/MWCNTs composite films with different MWCNTs contents

4　Conclusion

TiO_2/MWCNTs composite films were successfully prepared by a sol–gel hydrothermal method and EHD technology. The MWCNTs loading clearly influences the morphology of the thin films and the performance of the DSSCs. SEM shows that the addition of MWCNTs results in an increase in the pores of the film, and more pores are conducive to dye adsorption, electrolyte filling and charge transport. EIS analysis shows that proper MWCNTs loading enhances the transport of charge to the conductive glass, which reduces the recombination probability between the excited electrons and oxidized dye. Furthermore, the TiO_2/MWCNTs composite films with low loading result in an increased absorption intensity. As a result, a DSSC based on the CNT-0.12 (0.12%, in mass) photoanode and SnO_2/MWCNTs counter electrode achieves the highest conversion efficiency, *i.e.*, 5.80%, which is 30.6% higher than that of CNT-0. The conversion efficiency improvement is due to the rapid electron transportation in MWCNTs and increased dye adsorption.

References:

[1] HASANUZZAMAN M, RAHIM N A, SAIDUR R, et al. Energy savings and emissions reductions for rewinding and replacement of industrial motor[J]. Energy, 2011, 36(1): 233–240.

[2] O'REGAN B, GRÄTZEL M. A low-cost, high-efficiency solar cell based on dye-sensitized colloidal TiO_2 films[J]. Nature, 1991, 353(6346): 737

[3] LONGO C, FREITAS J, PAOLI M A D. Performance and stability of TiO_2/dye solar cells assembled with flexible electrodes and a polymer electrolyte[J]. J Photochem Photobio A, 2003, 159(1): 33–39.

[4] NAZEERUDDIN M K, KAY A, RODICIO I, et al. Conversion of light to electricity by cis-X2bis (2, 2'-bipyridyl-4, 4'-dicarboxylate) ruthenium (II) charge-transfer sensitizers (X= Cl-, Br-, I-, CN-, and SCN-) on nanocrystalline titanium dioxide electrodes[J]. J Am Chem Soc, 1993, 115(14): 6382–6390.

[5] LI J, WANG L, KONG X, et al. A simple and efficient method using polymer dispersion to prepare controllable nanoporous TiO_2 anodes for dye-sensitized solar cells[J]. Langmuir, 2009, 25(18): 11162–11167.

[6] MEHMOOD U, AL-AHMED A, AFZAAL M, et al. Enhancement of the photovoltaic performance of dye-sensitized solar cells by cosensitizing TiO_2 photoanode with uncapped PbS nanocrystals and ruthenizer[J]. IEEE J Photovolt, 2018, 8(2): 512–516.

[7] CHIU W H, LEE C H, CHENG H M, et al. Efficient electron transport in tetrapod-like ZnO metal-free dye-sensitized solar cells[J]. Energ Environ Sci, 2009, 2(6): 694–698.

[8] LI Z, ZHOU Y, SUN R, et al. Nanostructured SnO_2 photoanode-based dye-sensitized solar cells[J]. Chin Sci Bull, 2014, 59(18): 2122–2134.

[9] BHATTI K A, KHAN M I, SALEEM M, et al. Analysis of multilayer based TiO_2 and ZnO photoanodes for dye-sensitized solar cells[J]. Mater Res Express, 2019, 6(7): 075902.

[10] GAO C, LI X, LU B, et al. A facile method to prepare SnO_2 nanotubes for use in efficient SnO_2–TiO_2 core–shell dye-sensitized solar cells[J]. Nanoscale, 2012, 4(11): 3475–3481.

[11] SAURDI I, SHAFURA A K, MAMAT M H, et al. Electrical properties of TiO_2 at different deposition frequencies and their application in ZnO/TiO_2 based dye-sensitized solar cells[J]. AIP Conference Proceedings, 2018, 1963(1): 020036.

[12] MOJADDAMI M, MOHAMMADI M R, MADAAH HOSSEINI H R. Improved efficiency of dye-sensitized solar cells based on a single layer deposition of skein-like TiO_2 nanotubes[J]. J Am Ceram Soc, 2014, 97(9): 2873–2879.

[13] GU J, KHAN J, CHAI Z, et al. Rational design of anatase TiO_2 architecture with hierarchical nanotubes and hollow microspheres for high-performance dye-sensitized solar cells[J]. J Power Sources, 2016, 303: 57–64.

[14] BAKHSHAYESH A M, MOHAMMADI M R, DADAR H, et al. Improved efficiency of dye-sensitized solar cells aided by corn-like TiO_2 nanowires as the light scattering layer[J]. Electrochim Acta, 2013, 90: 302–308.

[15] HONG C K, JUNG Y H, KIM H J, et al. Electrochemical properties of TiO_2 nanoparticle/nanorod composite photoanode for dye-sensitized solar cells[J]. Curr Appl Phys, 2014, 14(3): 294–299.

[16] FAN K, ZHANG W, PENG T, et al. Application of TiO_2 fusiform nanorods for dye-sensitized solar cells with significantly improved efficiency[J]. J Phys Chem C, 2011, 115(34): 17213–17219.

[17] SAIFUDDIN N, RAZIAH A Z, JUNIZAH A R. Carbon nanotubes: A review on structure and their interaction with proteins[J]. J Chem, 2013: 8.

[18] BATMUNKH M, BIGGS M J, SHAPTER J G. Carbon nanotubes for dye-sensitized solar cells[J]. Small, 2015, 11(25): 2963–2989.

[19] YANG L, AN Y, DAI B, et al. Fabrication of carbon nanotube-loaded TiO_2@AgI and its excellent performance in visible-light photocatalysis[J]. Korean J Chem Eng, 2017, 34(2): 476–483.

[20] MEHMOOD U, MALAIBARI Z, RABANI F A, et al. Photovoltaic improvement and charge recombination reduction by aluminum oxide impregnated MWCNTs/TiO_2 based photoanode for dye-sensitized solar cells[J]. Electrochim Acta, 2016, 203: 162–170.

[21] LEGHRIB R, FELTEN A, PIREAUX J J, et al. Gas sensors based on doped-CNT/SnO_2 composites for NO_2 detection at room temperature[J]. Thin Solid Films, 2011, 520(3): 966–970.

[22] KIM T, SRIDHARAN I, ZHU B, et al. Effect of CNT on collagen fiber structure, stiffness assembly kinetics and stem cell differentiation[J]. Mater Sci Eng C, 2015, 49: 281–289.

[23] ARTUKOVIC E, KAEMPGEN M, HECHT D S, et al. Transparent and flexible carbon nanotube transistors[J]. Nano Lett, 2005, 5(4): 757–760.

[24] YAN D J, ZHU X D, MAO Y C, et al. Hierarchically organized CNT@TiO_2@Mn_3O_4 nanostructures for enhanced lithium storage performance[J]. J Mater Chem A, 2017, 5(32): 17048–17055.

[25] KILIC B, TURKDOGAN S, ASTAM A, et al. Preparation of carbon nanotube/TiO_2 mesoporous hybrid photoanode with iron pyrite (FeS_2) thin films counter electrodes for dye-sensitized solar cell[J]. Sci Rep, 2016, 6: 27052.

[26] YU J, FAN J, CHENG B. Dye-sensitized solar cells based on anatase TiO_2 hollow spheres/carbon nanotube composite films[J]. J Power Sources, 2011, 196(18): 7891–7898.

[27] DU P, SONG L, XIONG J, et al. Dye-sensitized solar cells based on anatase TiO_2/multi-walled carbon nanotubes composite nanofibers photoanode[J]. Electrochim Acta, 2013, 87: 651–656.

[28] JIN Z, ZHANG M, WANG M, et al. Metal selenides as efficient counter electrodes for dye-sensitized solar cells[J]. Accounts Chem Res, 2017, 50(4): 895–904.

[29] ZHANG J, WU W, ZHANG C, et al. Prussian-blue analog-derived Co_3S_4/MoS_2 porous nanocubes as enhanced Pt-free electrode catalysts for high-efficiency dye-sensitized solar cells[J]. Appl Surf Sci, 2019, 484: 1111–1117.

[30] MURUGADOSS V, PANNEERSELVAM P, YAN C, et al. A simple one-step hydrothermal synthesis of cobalt nickel selenide/graphene nanohybrid as an advanced platinum free counter electrode for dye sensitized solar cell[J]. Electrochim Acta, 2019, 312: 157–167.

[31] PAN Y, CHENYANG X U, HONG L, et al. Preparation and properties of carbon counter electrodes for dye-sensitized solar cells[J]. J Chin Ceram Soc, 2011, 39(12):1993–1996.

[32] WANG X, XIE Y, JIAO Y, et al. Carbon nanotubes *in situ* embedded with NiS nanocrystals outperform Pt in dye-sensitized solar cells: Interface improved activity[J]. J Mater Chem A, 2019, 7(17): 10405–10411.

[33] LIU Y X, LIU Q L, WANG X Y, et al. SnO_2/carbon naotubes nanocomposite as Pt-free counter electrode used in dye-sensitized solar cells[J]. J Funct Mater, 2019, 50(1): 144–148.

[34] CAI J, CHEN Z, LI J, et al. Enhanced conversion efficiency of dye-sensitized solar cells using a CNT-incorporated TiO_2 slurry-based photoanode[J]. AIP Adv, 2015, 5(2): 027118.

[35] GHARTAVOL H M, MOHAMMADI M R, AFSHAR A, et al. Efficient dye-sensitized solar cells based on CNT-derived TiO_2 nanotubes and Nb-doped TiO_2 nanoparticles[J]. Rsc Adv, 2016, 6(103): 101737–101744.

[36] WANG Q, MOSER J E, GRÄTZEL M. Electrochemical impedance spectroscopic analysis of dye-sensitized solar cells[J]. J Phys Chem B, 2005, 109(31): 14945–14953.

[37] DU P, SONG L, XIONG J, et al. Dye-sensitized solar cells based on anatase TiO_2/multi-walled carbon nanotubes composite nanofibers photoanode[J]. Electrochim Acta, 2013, 87: 651–656.